Mineralogical Magazine (2019), **83**, 57–69
doi:10.1180/mgm.2018.147

CAMBRIDGE UNIVERSITY PRESS

Article

Quantitative Raman calibration of sulfate-bearing polymineralic mixtures: a S quantification in sedimentary rocks on Mars

Chloé Larre[1]*, Yann Morizet[1], Catherine Guillot-Deudon[1,2], Fabien Baron[1] and Nicolas Mangold[1]

[1]Université de Nantes, Faculté des Sciences et Techniques, Laboratoire de Planétologie et Géodynamique (LPG), UMR CNRS 6112, 2 rue de la Houssinière, 44322 Nantes, France; and [2]IMN, Institut des Matériaux Jean Rouxel de Nantes, UMR CNRS 6502, 2 rue de la Houssinière, 44322 Nantes, France

Abstract

The NASA 2020 Mars mission is a Curiosity-type rover whose objective is to improve the knowledge of the geological and climatic evolution of Mars and to collect rock samples for return to Earth. The new rover has a payload of seven instruments including the SuperCam instrument which consists of four tools including a Raman spectrometer. This Raman device will be non-destructive and will analyse the surface remotely in order to determine the mineralogy of rocks and, by extent, to detect and quantify major elements such as sulfur. Sulfur has been detected as sulfate (Ca,Mg,Fe-sulfates) in sedimentary rocks. This element is difficult to quantify using the laser ablation tool of the ChemCam instrument on-board the Curiosity rover.

We propose a Raman calibration to constrain the sulfur abundance in polymineralic mixtures. We acquired Raman signatures on binary and ternary mechanical mixtures containing Ca and Mg sulfates, mixed with natural silicate minerals supposed to be relevant to basaltic-sedimentary rocks at the surface of Mars: olivine, clinopyroxene, orthopyroxene and plagioclase. Using the Voigt function to process the Raman spectra from samples extracted from our mixtures allows us to calculate the initial proportions of our preparations of Ca and Mg sulfates. From these simulations, calibration equations have been provided allowing us to determine sulfate proportions ($CaSO_4$ and $MgSO_4$) in a mixture with basaltic minerals. With the presented calibration, S can be quantified at a lower limit of 0.7 wt.% in Martian soil.

Keywords: Raman spectroscopy, S abundance, sulfates, sedimentary rocks, Mars

(Received 8 January 2018; accepted 19 July 2018)

Introduction

One of the main objectives of both orbital and landed Mars missions is the mineralogical characterisation of the igneous and sedimentary rocks in order to constrain past geological processes such as the early volcanism and aqueous alteration. So far, many types of igneous rocks have been detected at the surface of Mars with basaltic rocks being the most abundant (e.g. Bandfield *et al.*, 2000; McSween *et al.*, 2009; Taylor and McLennan, 2009; Ody, 2012; Baratoux *et al.*, 2013; Sautter *et al.*, 2016; Cousin *et al.*, 2017), though recently the Curiosity rover and the orbital spectrometer CRISM have discovered rocks that are more felsic and alkali-rich including trachyte, andesite, diorite and putative granitoids (Wray *et al.*, 2013; Stolper *et al.*, 2013; Sautter *et al.*, 2015; Mangold *et al.*, 2016). These magmatic rocks have been altered into diverse minerals such as clays (various smectites, kaolinite and chlorite-group minerals) and sulfates (Ca-, Fe-, Mg-sulfates), which are commonly detected in sediment layers overlying the igneous bedrock or in crustal outcrops exhumed by impact craters (e.g. Arvidson *et al.*, 2005; Squyres and Knoll, 2005; Poulet *et al.*, 2005; Gendrin *et al.*, 2005; Elhmann *et al.*, 2013, Carter *et al.*, 2013).

The Curiosity rover currently analyses rocks and soils on Mars using Laser Induced Breakdown Spectroscopy (LIBS) (Maurice *et al.*, 2012; Wiens *et al.*, 2012; Meslin *et al.*, 2013; Maurice *et al.*, 2016; Cousin *et al.*, 2017; Mangold *et al.*, 2017). The LIBS equipment enables the detection and quantification of all major elements (e.g. Si and Al) and the detection of volatiles and halogens (C-H-O-N-P-S-F-Cl). However, the detection of these latter elements is difficult with this method because of the high excitation energies, their peak positions near the instrument limit, and the coupling of different major-element rays (e.g. Sallé *et al.*, 2004; Clegg *et al.*, 2007). This results for some in varying detection levels and lack of quantification. In particular, the detection limit for S is 5 to 10 wt.% S (Wiens *et al.*, 2012). The quantitative determination of S is of prime interest, as this element is known to be fundamental for Mars evolution (King and McLennan 2010).

In the Mars 2020 mission, the SuperCam analytical equipment will include Raman and infrared spectrometers in addition to the LIBS instrument similar to the ChemCam instrument on-board Curiosity (Fouchet *et al.*, 2016; Wiens *et al.*, 2016; Ollila *et al.*, 2017). Relevant interpretations of Raman spectra in this study will require the acquisition of laboratory data under similar analytical conditions of the on-board Raman spectrometer. Although Raman spectroscopy is nominally non-quantitative with relevant calibration, it can be used for quantifying S at low concentrations

***Author for correspondence:** Chloé Larre, Email: chloe.larre@univ-nantes.fr
Associate Editor: Andrew Christy
Cite this article: Larre C., Morizet Y., Guillot-Deudon C., Baron F. and Mangold N. (2019) Quantitative Raman calibration of sulfate-bearing polymineralic mixtures: a S quantification in sedimentary rocks on Mars. *Mineralogical Magazine*, **83**, 57–69. https://doi.org/10.1180/mgm.2018.147

(thousands of ppm) owing to the high Raman activity of S-bearing molecular groups (Morizet *et al.*, 2017).

Previous studies have focused on the quantification of volatile species (H_2O, CO_2 and SO_4^{2-}) in silicate glasses with application to Earth volcanism (Zajacz *et al.*, 2005; Mercier *et al.*, 2009; Le Losq *et al.*, 2012; Morizet *et al.*, 2013*a*,*b*, 2017). However, up to now, only the quantification of individual mineral species in polymineralic mechanical mixtures have been addressed using Raman spectroscopy (Kontoyannis *et al.*, 1997; Jehlicka *et al.*, 2009; Noguchi *et al.*, 2009; Kriskova *et al.*, 2013; Culka *et al.*, 2014). Jehlicka *et al.* (2009) have shown the possibility of quantifying multi-component mixtures with a portable micro-Raman spectrometer, while in Kriskova *et al.* (2013) and Noguchi *et al.* (2009) only polymineralic mixtures with carbonates have been studied. Kontoyannis *et al.* (1997) have established a calibration for carbonates mixed with gypsum using Raman spectroscopy, but have not applied this to mineralogical mixtures representative of Martian mineralogy.

In the present work, we propose a calibration for quantifying the sulfate content (thereby also the elemental sulfur content) in polymineralic mixtures. This calibration will be used for quantifying S as sulfates on the surface of Mars with the Raman spectrometer of SuperCam. Several mixtures of sulfates (Ca-sulfate, Mg-sulfate) with silicate minerals (i.e. pyroxenes, olivine and plagioclase) were prepared in order to reproduce sulfate-bearing Martian-like sedimentary rocks. These mixtures were analysed by Raman spectroscopy. The equations derived from the calibration curves are then used to quantify sulfates in these mixtures. Finally, we discuss the potential of this method to quantify S carried by sulfates in the Martian soil and rocks.

Methods

Polymineralic mixtures preparation

Polymineralic mixtures were prepared from Ca-sulfate ($CaSO_4 2H_2O$) and Mg-sulfate ($MgSO_4 \cdot nH_2O$) synthetic powders and silicate minerals selected from natural rocks. Pyroxenes and olivine were extracted from a xenolith collected at the Maar du Borée, Massif Central, France, and plagioclase from Stillwater norite (Montana, USA). The compositions of the minerals selected for this study are reported in Table 1. Olivine is Mg-rich (forsterite, $Si_{1.00}Fe_{0.18}Mg_{1.78}Na_{0.01}O_4$). The two pyroxenes have compositions close to enstatite ($Si_{1.85}Al_{0.16}Fe_{0.16}Mg_{1.62}Ca_{0.02}Na_{0.02}O_6$) and augite end-members ($Si_{1.78}Al_{0.23}Fe_{0.09}Mg_{0.95}Ca_{0.57}Na_{0.11}O_6$). The plagioclase is Ca-rich and has a composition close to the anorthite end-member ($Si_{2.21}Al_{1.76}Fe_{0.01}Mg_{0.01}Ca_{0.85}Na_{0.1}O_8$). Natural silicate minerals were crushed in a steel mortar with a pestle and crushed again in an agate mortar. Ethanol was added during crushing to clean the samples.

Mixtures of different silicate minerals and sulfates were prepared and mixed together. The resulting powder was not sieved because the grain size does not exceed 50 μm using this grinding procedure (see Fig. 1*a*). Several samples at various sulfate proportions were prepared: $WF_{gypsum} = 0.20$, 0.10, 0.05, 0.03, 0.01 and $WF_{Mg\text{-}sulfate}$=0.20, 0.10, 0.05 and 0.03; where WF represents the Weight Fraction of sulfates. Ternary mixtures were prepared with Ca-sulfate, clinopyroxene and olivine. Gypsum, clinopyroxene and olivine concentrations in mixtures were, respectively: $WF_{gypsum} = 0.20$, 0.10 and 0.05, $WF_{clinopyroxene} = 0.40$, 0.40 and 0.45, $WF_{olivine} = 0.40$, 0.50 and 0.50. The sulfate concentrations investigated are consistent with the abundances of these minerals estimated locally in evaporites at Meridiani Planum (McLennan *et al.*, 2005) or in fluvio-lacustrine sedimentary rocks at Gale crater (Vaniman *et al.*, 2017) on Mars.

We also prepared ternary mixtures in order to reproduce the suggested Martian surface mineralogy in a more realistic system: sulfates mixed with silicate minerals resulting from basalt alteration (Carter *et al.*, 2013; Forni *et al.*, 2015; Cousin *et al.*, 2017; Mangold *et al.*, 2017). The resulting powders were then pressed into pellets (Fig. 1*a*). Pressures used were between 5000 and 9000 kg/cm^2 to create pellets 7 and 10 mm diameter, respectively.

No mixtures with basaltic glasses were made due to the difficulty of establishing a Raman calibration for a glass component mixed with a crystal because of the large difference on the Raman spectrum intensity. Further work could be undertaken on this kind of mixture to constrain better the S abundance of Mars.

Raman spectroscopy

The non-destructive nature of the Raman analyses permits mineralogical characterisation (e.g. Reynard *et al.*, 2012) of the Martian rocks without any sample preparation. The Raman spectroscopy uses a laser with a specific wavelength that excites the molecules (Brawer and White, 1975; Mysen and Virgo, 1980*a*,*b*; McMillan, 1984; Rossano and Mysen 2012; Rull, 2012). This excitation produces a Raman shift (i.e. the wavenumber difference between the signal from the laser and the response of excited molecules; Delhaye and Dhamelincourt 1975; Hoehse *et al.*, 2009; Dubessy *et al.*, 2012). The strongest signatures received and detected by the Raman spectrometer are called ν_1 signatures and correspond to the symmetric stretching of the molecules excited by the laser (Rossano and Mysen 2012; Rull 2012).

Raman spectra for each pellet were acquired using a Jobin-Yvon Labram HR800 spectrometer equipped with a solid-state laser diode operating at 532 nm. A 20× Olympus objective was used. A 785 nm solid-state laser has also been used for one sample (GPG80, plagioclase-gypsum mixture with WF_{gypsum} = 0.20) to circumvent fluorescence. Spectra are acquired with a 300 grooves/mm grating with a 3 cm^{-1} spectral resolution. The output power of the laser was set to 74 mW for Ca-sulfate mixtures and 50 mW for Mg-sulfate. For binary mixtures, we did not use the confocal mode (with a hole calibrated around

Table 1. Origins and compositions of basaltic minerals (olivine, pyroxenes and plagioclase, determined by scanning electron microscopy analysis) and sulfates used in this investigation.

Mineral	Origin	Formula
Olivine	Forsterite from Maar de Borée, Massif Central, France	$Si_{1.00}Fe_{0.18}Mg_{1.78}Na_{0.01}O_4$
Clinopyroxene	Augite from Maar de Borée, Massif Central, France	$Si_{1.78}Al_{0.23}Fe_{0.09}Mg_{0.95}Ca_{0.57}Na_{0.11}O_6$
Orthopyroxene	Enstatite from Maar de Borée, Massif Central, France	$Si_{1.85}Al_{0.16}Fe_{0.16}Mg_{1.62}Ca_{0.02}Na_{0.02}O_6$
Plagioclase	Anorthite from a norite of Stillwater, Montana, USA	$Si_{2.21}Al_{1.76}Fe_{0.01}Mg_{0.01}Ca_{0.85}Na_{0.16}O_8$
Gypsum	Synthetic calcium sulfate dehydrated from MERCK, Germany	$CaSO_4 \cdot (2H_2O)$
Mg-sulfate	Synthetic magnesium sulfate hydrated from LABOSI, France	$MgSO_4 \cdot (nH_2O)$

https://doi.org/10.1180/mgm.2018.147 Published online by Cambridge University Press

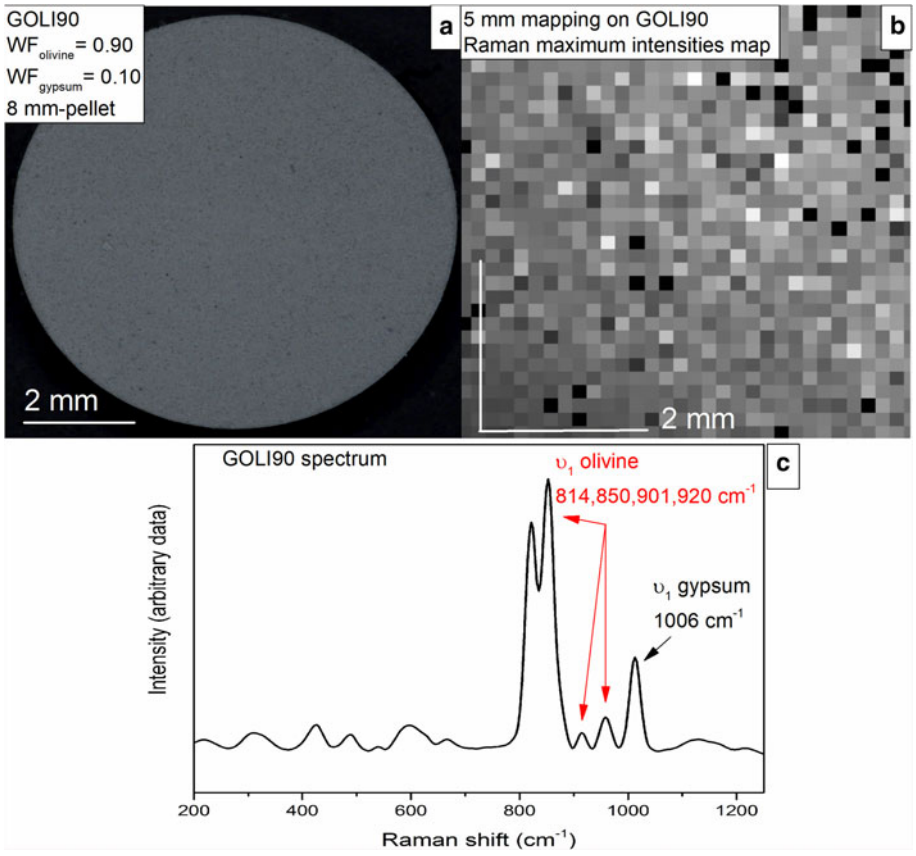

Fig. 1. (*a*) Pellet of a 90/10 mixture of olivine (weight fraction $WF_{olivine} = 0.90$) and gypsum ($WF_{gypsum} = 0.10$) named GOLI90; (*b*) 5 mm mapping of spectrum intensities acquired by Raman spectroscopy showing the homogeneity of GOLI90; and (*c*) the average spectrum issued from the 5 mm mapping of GOLI90 with ν_1 peaks (symmetric stretching mode of SiO_4 and SO_4 molecules) of olivine and gypsum reported.

50 μm) and the hole was fixed at 200 μm, however, ternary mixtures were analysed in a confocal mode due to fluorescence problems (Panzcer *et al.*, 2012) in the non-confocal configuration.

The acquisition time varied from 3 to 10 s and 3 repetitive scans were made on each point. Background subtraction for each spectrum has been applied following the procedure of Tarcea and Popp (2012): a fit of polylines (i.e. multiple lines added to create a baseline under the spectrum) was made for each spectrum to establish a baseline correction in order to measure areas and intensities for each peak. Peak intensity and area were determined on normalised spectra to the same acquisition time length (10 or 15 s). Details of the analytical conditions are reported in the Supplementary Material (Table S1).

Mapping of a large 5 mm by 5 mm area (Fig. 1*b*) was conducted on each pellet with a spot size of ~1.6 μm. Each analysis was performed every 150 μm. This mapping results in 1024 spectra representing the mixture analysed. As the grain size did not exceed 50 μm, possible coupling of the same crystal analysis is expected; this phenomenon would have occurred for every crystal as we have presumed that the mixture has a homogeneous grain size (Fig. 1*a*). Then, an average of these spectra, that considers the previous artefact, is computed to obtain a single Raman spectrum representative of the analysed mixture (Fig. 1*c*).

The effect of polarisation was also investigated on Raman spectra of pure minerals. We have observed that the spectrum intensity is modified when the acquisition angle on the crystal is changed, which is consistent with the results of Bremard *et al.* (1986) and Rull (2012), where polarisation effects have been observed and measured when changing crystal orientation. Nevertheless, we assumed that the polarisation effect is averaged out by the large mapping procedure adopted and considering that crystals in the pellet have all possible crystallographic orientations from a statistical point of view.

Mineral Raman spectra

The Raman spectra of individual minerals used in this study are in Fig. 2. The pure gypsum Raman spectrum (Fig. 2*a*) exhibits several peaks with low intensities in the 400–700 cm^{-1} region corresponding to the symmetric (400–500 cm^{-1}) and antisymmetric (600–700 cm^{-1}) bending vibrations of SO_4 molecules (ν_2 and ν_4). The strong peak at 1006 cm^{-1} corresponds to the symmetric stretching vibration (or ν_1) of S–O bonds in SO_4 molecular groups (Knittle *et al.*, 2001; Buzgar *et al.*, 2009; Bishop *et al.*, 2014). Peaks observed in the highest frequency region (>1100 cm^{-1}) are attributed to antisymmetric stretch vibrations (ν_3) of SO_4 and have a weak Raman activity.

In common with gypsum, the principal symmetric ν_1 vibration of Mg-sulfate is identified in Fig. 2*b* around 1040 cm^{-1} (Buzgar *et al.*, 2009). Antisymmetric bending and stretching of SO_4 molecules are observed at 620 and 1110 cm^{-1}, respectively.

The Raman spectrum of olivine (Fig. 2*c*) shows two strong peaks above 800 cm^{-1}, followed by two less intense peaks above 900 cm^{-1}, which are attributed to the symmetric stretch of the Si–O bonds of SiO_4 tetrahedrons (Chopelas 1991; Kolesov and Tanskaya 1996; Kolesov and Geiger 2004; Kuebler *et al.*, 2006; McKeown *et al.*, 2010).

Plagioclase Raman spectrum shown in Fig. 2*d* exhibits a strong peak around 500 cm^{-1} attributed to the ν_1 of Al_2O_3 or SiO_4 tetrahedrons in the tectosilicate structure (Sharma *et al.*, 1983; Freeman *et al.*, 2008). Peaks identified at higher wavenumbers correspond to the ν_3 vibrations for these tetrahedrons.

https://doi.org/10.1180/mgm.2018.147 Published online by Cambridge University Press

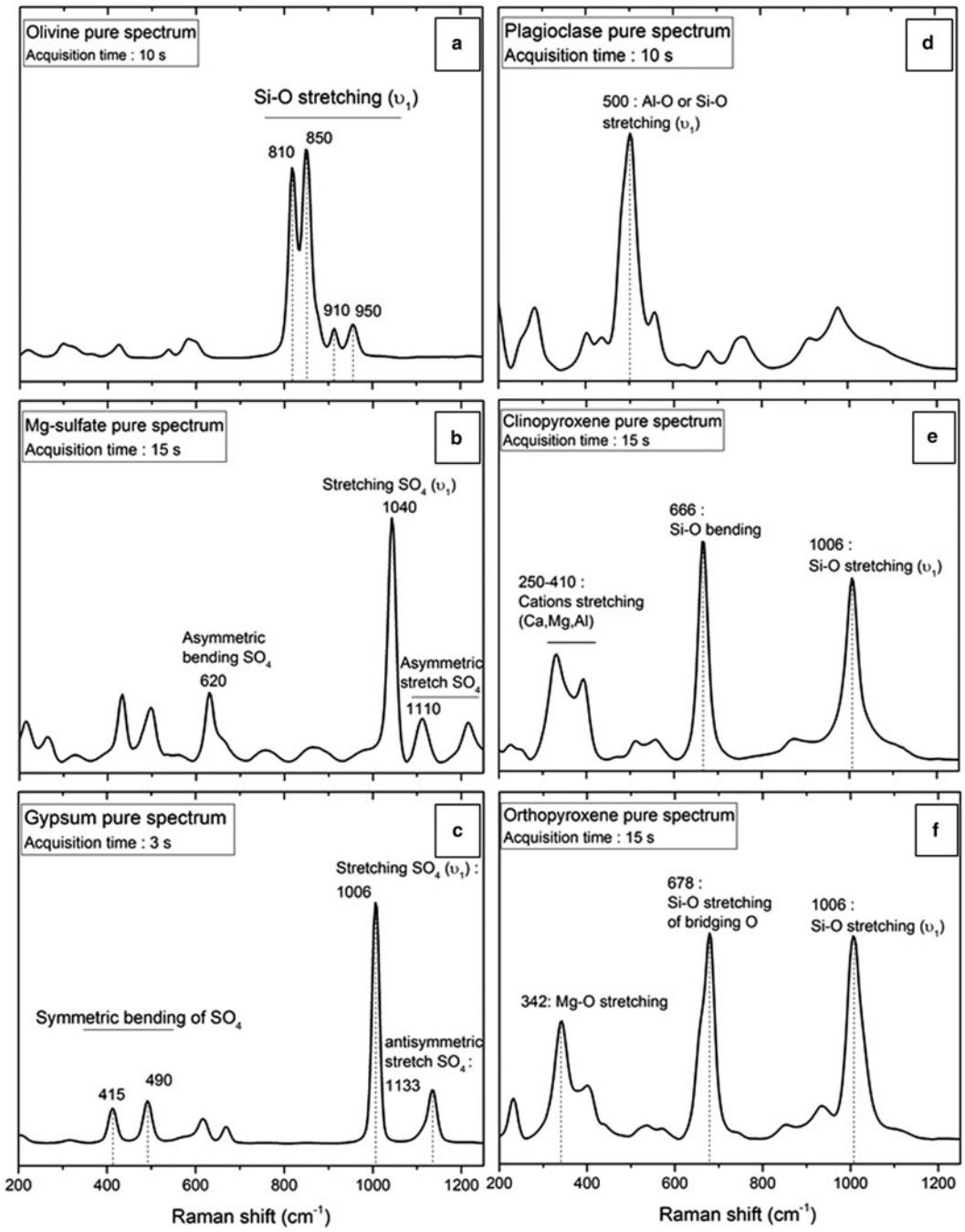

Fig. 2. Polymineralic Raman spectra of pure samples with acquisition time for (*a*) olivine; (*b*) Mg-sulfate; (*c*) gypsum; (*d*) plagioclase; (*e*) clinopyroxene; and (*f*) orthopyroxene. Significant peaks for each mineral are shown. For peak assignments see Table 2.

Pyroxene spectra shown in Figs 2*e* and 2*f* are similar in the high-frequency region (>600 cm^{-1}) where bending and stretching vibrations of SiO_4 tetrahedrons are observed, for signatures around 660 and 1006 cm^{-1} respectively. At low frequency, in the 200–400 cm^{-1} region, it is possible to discriminate clinopyroxene from orthopyroxene, which does not present the same peak intensities. In this region, vibrations related to Fe, Ca and Mg molecular environments are responsible for the observed peaks (Sharma *et al.*, 1983; Huang *et al.*, 2000; Wang *et al.*, 2001; Prencipe *et al.*, 2011; Tribaudino *et al.*, 2012). Specific peak assignments for each mineral investigated are described in Table 2.

Analytical conditions useable for the SuperCam instrument

The new rover for the 2020 Mars mission will use a laser-pulse Raman spectrometer with a 532 nm solid-state laser (Ollila *et al.*, 2017; Wiens *et al.*, 2016). The rover will target rocks and soil from several meters away and with a resolution on the order of 10 cm^{-1} (Wiens *et al.*, 2016).

Knowing those conditions, we performed several tests to analyse the pellets. A map size of 5 mm by 5 mm was necessary to reproduce the mineral mixtures adequately. Using a 2×2 or 3×3 mm map size was not sufficient to retrieve the initial mineral proportions in the mixture. Furthermore, the 5×5 mm size map is also consistent with the analytical conditions for the 2020 rover,

https://doi.org/10.1180/mgm.2018.147 Published online by Cambridge University Press

Table 2. Specific peak assignments for each mineral used in this study*.

Raman shift (cm^{-1})	Mode assignments	Raman shift (cm^{-1})	Mode assignments
Orthopyroxene [1], [2], [3], [4]		Olivine [5], [6], [7], [8]	
225–325	Fe–O octahedron	820	Si–O ν_1
375–490	Mg–O octahedron	850	Si–O ν_1
650–750	Si–O ν_3[c]	914	Si–O ν_3
800–1100	Si–O ν_1[a]	950	Si–O ν_3
Clinopyroxene [1], [2], [3], [4]		Plagioclase [9], [3]	
230 and 327	*M*–O** stretching	200–400	Lattice modes
255 and 360	Ca–O stretching	420–503	Al–O or Si–O ν_1
393	Mg–O stretch	900–1000	Si–O–Al ν_3
665	Si–O–Si ν_2[b]	>1000	Si–O–Si ν_3
1010	Si–O ν_1		
Gypsum [10], [11], [12]		Mg-sulfate [11]	
400–500	SO_4 ν_2	400–600	SO_4 ν_2
600–700	SO_4 ν_4[d]	620	SO_4 ν_4
1006	SO_4 ν_1	1040	SO_4 ν_1
>1100	SO_4 ν_3	1050–1150	SO_4 ν_3

*Principal peaks observed in spectra are described according to: [1] Huang *et al.* (2000); [2] Prencipe *et al.* (2011); [3] Sharma *et al.* (1983); [4] Wang *et al.* (2001); [5] Chopelas (1991); [6] Kolesov and Tanskaya (1996); [7] Kolesov and Geiger (2004); [8] McKeown *et al.* (2010); [9] Freeman *et al.* (2008); [10] Bishop *et al.* (2014); [11] Buzgar *et al.* (2009); and [12] Knittle *et al.* (2001).
**'*M*' = different metal cations present in the chemical structure of the mineral (Buzgar *et al.*, 2009).
[a]ν_1: Symmetric stretch; [b]ν_2: symmetric bending; [c]ν_3: antisymmetric stretch; [d]ν_4: antisymmetric bending.

which will have a large analytical area. The adopted laboratory analytical conditions (i.e. focus 20×, 300 grooves/mm grating and non-confocal mode) were optimised to obtained spectra that could be compared to the Raman spectra that will be acquired by SuperCam.

Calibration method

The calibration method in the present investigation is similar to that used by Kontoyannis *et al.* (1997), Noguchi *et al.* (2009) and Kristova *et al.* (2013). Our method is based on the spectral deconvolution of the Raman spectrum of the pure minerals investigated in the previous section. For example, to establish a calibration on a gypsum–olivine mixture, the pure spectrums of gypsum and olivine are treated individually. The spectrum treatment consists of extracting peak information using subsequent deconvolution. As we are analysing crystallised species, we expect the Raman signature to have a pure Lorentzian shape; however, a contribution of a Gaussian component in addition to the Lorentzian signal has been observed. This is probably caused by intrinsic crystal defaults. Therefore, we used a Voigt simulation (i.e. a mix of Gaussian and Lorentzian deconvolution) which provides better simulations of our spectra. The simulation equation of a Voigt deconvolution is given below (Eq. 1):

$$y = y_0 + A\,\frac{2\ln 2}{\pi^{\frac{3}{2}}}\times\frac{W_L}{W_G^2}\times\int_{-\infty}^{\infty}\frac{e^{-t^2}}{\left(\sqrt{\ln 2}\times\frac{W_L}{W_G}\right)^2+\left(\sqrt{4\ln 2}\times\frac{x-x_c}{W_G}-t\right)^2}\,dt \quad (1)$$

Where y_0 and y are the intensity after a baseline correction of the spectrum and the intensity for the simulated peak, respectively. The parameter A represents the simulated area and W_G and W_L are, respectively, the Gaussian and Lorentzian widths for a given peak. The x parameter is the position in cm^{-1}; where x is the Raman shift and x_c is the derived peak position simulated in cm^{-1}. Finally, in equation 1, t is the time component, though as the Raman spectra are not time-dependent, t is set to 0. All the peaks simulated for pure mineral spectra, with their specific parameters (width, position and area) are reported in Supplementary Table S1. For clarity, simulations of silicate and sulfate minerals pure spectra are also only shown in the Supplementary material (Fig. S1).

Due to the strong overlapping between the different spectral lines in the recovered average Raman spectrum for each pellet, it was not possible to perform the simulation of all the identified peaks for the pure spectrum of the minerals reported in Table 2. For instance, clinopyroxene has a main peak at 1006 cm^{-1} comparable to the one in the gypsum Raman spectrum. Therefore, simulating those two peaks in the average mixed spectrum is complicated by their proximity and a relevant simulation could not be achieved. Hence, for each species, we have selected peaks that are distinct in their position. These are indicated in Table 3.

The protocol to simulate Raman peaks is described fully in previous investigations and is used routinely for the quantification of volatiles species in silicate glasses (Mysen and Virgo 1980*a*,*b*; Mercier *et al.*, 2009; Morizet *et al.*, 2013*a*, 2017). First, we have fixed the peak position and widths (Gaussian and Lorentzian), leaving only the peak area optimised. The position is then optimised as we observed slight variations in the peak position in our mixtures compared to the position derived from the acquired pure spectrum. These variations could be due to the dependence of the Raman signature on crystal orientation or unaccounted for chemical heterogeneity. The Gaussian and Lorentzian widths are also optimised to better fit our simulations. This procedure is repeated several times until the chi-square (χ^2 parameter representing the robustness of the fit) is the lowest possible and the residuals are small (see Fig. 3).

With parameters extracted from simulations, we were able to calculate the mixed proportions present in the analysed pellet. We determined a ratio R between the simulated area for the peak of the mixed spectrum and that of the pure spectrum such as:

$$R = \frac{A_{\text{mixture}}}{A_{\text{pure}}} \quad (2)$$

In equation 2, A represents the area determined with a Voigt simulation for a same peak for the mixture (A_{mixture}) and the pure Raman spectrum (A_{pure}). This method differs from previous Raman calibrations studies of Kontoyannis *et al.* (1997) and Kristova *et al.* (2013) where peak intensities were chosen instead of areas. As we observed several variations in intensity and peak positions between pure spectra and the average spectra of the mixtures, we consider that using peak areas averaged out every possible variation between acquisitions with the 300 grooves/mm grating. The ratios are then normalised to obtain the result as a weight fraction (WF). This proportion is then assimilated to a coefficient '*a*':

$$a = \frac{\Sigma A_{\text{gypsum}}}{\Sigma A_{\text{mineral}}} \quad (3)$$

with A being peak areas for gypsum (A_{gypsum}) and for mineral in the mixture (A_{mineral}). For the ternary mixtures with more than two peaks simulated for one mineral, A_{mineral} is entirely summed

https://doi.org/10.1180/mgm.2018.147 Published online by Cambridge University Press

Table 3. Samples prepared in this study for binary and ternary mixtures with sulfates (Ca and Mg) and basaltic minerals (i.e olivine, orthopyroxene, clinopyroxene and plagioclase). For each mixture the simulated peak is given, followed by the resulting calibration equation.*

Sample name	WF theoretical	WF calculated	*a*	Sample name	WF theoretical	WF calculated	*a*
Olivine–Gypsum				Orthopyroxene–Gypsum			
Peak simulated: 914 and 1006 cm^{-1}				Peak simulated: 230 and 491 cm^{-1}			
Calibration equation: $a = 81.36 \times WF_{sulfate\ theoretical}$				Calibration equation: $a = 8.23 \times WF_{sulfate\ theoretical}$			
GOLI80	0.80–0.20	0.79(0.08)–0.21(0.01)	17.21(3.20)	GOPX80	0.80–0.20	0.85(0.04)–0.15(0.03)	1.52(0.01)
GOLI90	0.90–0.10	0.91(0.01)–0.09(0)	6.55(0.36)	GOPX90	0.90–0.10	0.89(0.03)–0.11(0.04)	0.99(0.12)
GOLI95	0.95–0.05	0.94(0.01)–0.06(0)	4.04(0.22)	GOPX95	0.95–0.05	0.94(0.02)–0.06(0.05)	0.51(0.01)
GOLI97	0.97–0.03	0.97(0.02)–0.03(0.04)	1.87(0.88)	GOPX97	0.97–0.03	0.96(0.01)–0.04(0.08)	0.34(0.35)
GOLI99	0.99–0.01	0.99(0)–0.01(0)	0.76(0.08)	GOPX99	0.99–0.01	0.98(0.01)–0.02(0.05)	0.19(0.23)
Clinopyroxene–Gypsum				Plagioclase–Gypsum			
Peak simulated: 362 and 412 cm^{-1}				Peak simulated: 504 and 1006 cm^{-1}			
Calibration equation: $a = 1.93 \times WF_{sulfate\ theoretical}$				Calibration equation: $a = 59.83 \times WF_{sulfate\ theoretical}$			
GCPX80	0.80–0.20	0.82(0.02)–0.18(0.02)	0.40(0.49)	GPG80	0.80–0.20	0.83(0.01)–0.17(0.01)	1.19(0.02)
GCPX90	0.90–0.10	0.92(0.01)–0.08(0.03)	0.15(0.69)	GPG90	0.90–0.10	0.90(0.03)–0.10(0.01)	6.24(0.89)
GCPX95	0.95–0.05	0.93(0)–0.07(0.01)	0.13(0.38)	GPG95	0.95–0.05	0.95(0.01)–0.05(0)	2.75(0.10)
GCPX97	0.97–0.03	0.96(0.01)–0.04(0.06)	0.07(0.54)	GPG97	0.97–0.03	0.98(0.01)–0.02(0.01)	1.17(0.04)
GCPX99	0.99–0.01	0.99(0)–0.01(0)	0.02(0.42)	GPG99	0.99–0.01	0.98(0)–0.02(0)	1.15(0.01)
Olivine–Clinopyroxene–Gypsum							
Peak simulated: 947–310/328/359/384–485							
Calibration equation: $a = 1.71 \times W_{sulfate\ theoretical}$							
GOLCX80	0.40–0.40–0.20	0.35(0.27)–0.50(0.01)–0.15(0.06)	0.35(0.05)				
GOLCX90	0.50–0.40–0.10	0.49(0.16)–0.35(0.06)–0.05(0.03)	0.15(0.03)				
GOLCX95	0.50–0.45–0.05	0.39(0.17)–0.44(0.07)–0.03(0.03)	0.07(0.02)				
Orthopyroxene–Mg-sulfate				Olivine–Mg-sulfate			
Peak simulated: 330/370/400–1040 cm^{-1}				Peak simulated: 950 and 1040 cm^{-1}			
Calibration equation: $a = 2.19 \times WF_{sulfate\ theoretical}$				Calibration equation: $a = 5.26 \times WF_{sulfate\ theoretical}$			
MgOPX80	0.80–0.20	0.82(0.02)–0.18(0.02)	0.43(0.02)	MgOLI80	0.80–0.20	0.84(0.05)–0.16(0.09)	0.90(0.19)
MgOPX90	0.90–0.10	0.89(0.01)–0.11(0.02)	0.25(0)	MgOLI90	0.90–0.10	0.86(0.02)–0.14(0.03)	0.81(0.03)
MgOPX95	0.95–0.05	0.90(0.01)–0.10(0.02)	0.20(0)	MgOLI95	0.95–0.05	0.94(0.03)–0.06(0.19)	0.30(0.59)
MgOPX97	0.97–0.03	0.96(0)–0.04(0.01)	0.08(0)	MgOLI97	0.97–0.03	0.95(0.02)–0.05(0.20)	0.23(0.63)
Plagioclase–Mg-sulfate				Clinopyroxene–Mg-sulfate			
Peak simulated: 750 and 1113 cm^{-1}				Peak simulated: 666/1006 and 1040 cm^{-1}			
Calibration equation: $a = 2.88 \times WF_{sulfate\ theoretical}$				Calibration equation: $a = 1.05 \times WF_{sulfate\ theoretical}$			
MgPG80	0.80–0.20	0.86(0.04)–0.14(0.09)	0.51(0.15)	MgCPX80	0.80–0.20	0.82(0)–0.18(0.04)	0.19(0.01)
MgPG90	0.90–0.10	0.91(0.03)–0.09(0.12)	0.33(0.21)	MgCPX90	0.90–0.10	0.87(0)–0.13(0.03)	0.14(0.01)
MgPG95	0.95–0.05	0.93(0.01)–0.07(0.07)	0.23(0.11)	MgCPX95	0.95–0.05	0.94(0)–0.06(0.04)	0.06(0.01)
MgPG97	0.97–0.03	0.93(0.02)–0.07(0.06)	0.22(0.10)	MgCPX97	0.97–0.03	0.96(0)–0.04(0.03)	0.03(0.01)

*Notes: $WF_{theroetical}$, $WF_{calculated}$ = theoretical and calculated weight fractions, respectively; *a* = coefficient. Errors related to calculations are reported in brackets next to $WF_{calculated}$ and '*a*' coefficient.

in the denominator. Examples of pure mineral spectra and mixture deconvolutions are provided in the Supplementary Fig. S1.

Results

Binary and ternary mixtures with Ca-sulfate

A typical example of the spectral treatment is shown in Fig. 3. In Fig. 3*a* Raman spectra has been collected that represents olivine and gypsum mixtures with $WF_{gypsum} = 0.2$, 0.1, 0.05 and 0.01. The Raman spectra obtained for the mixtures with other minerals (pyroxenes and plagioclase) are reported in Supplementary Fig. S2. In Fig. 3*a*, it can be observed that the peak intensity for ν_1 gypsum at 1006 cm^{-1} increases with increasing the proportion of gypsum in the mixture. For instance, in GOLI80 $WF_{gypsum} = 0.20$ (see Table 3 for theoretical WF of each mixture), the 1006 cm^{-1} symmetric stretch peak is more intense as compared to the one in GOLI90 ($WF_{gypsum} = 0.10$). For these two mixtures, the measured intensity in the SO_4 vibrations peak is twice for GOLI80 as compared to the one in GOLI90, which appears to be consistent with the prepared compositions (Table 3). Although the gypsum content in the GOLI99 mixture is extremely low ($WF_{gypsum} = 0.01$), the peak at 1006 cm^{-1} is still detected because of the strong Raman activity of symmetric stretch of the S–O bonds in SO_4 molecular groups in gypsum (see Fig. 3*a*).

We chose to simulate three different peaks in the 890–1100 cm^{-1} region and located at 914, 958 for olivine and 1006 cm^{-1} for gypsum (Fig. 3). For olivine mixtures, relevant results were obtained when considering two Raman peaks identified in Table 2: 914 cm^{-1} for olivine and 1006 cm^{-1} for gypsum. In order to avoid contribution of the 1006 cm^{-1} gypsum peak over the 950 cm^{-1} of olivine (see on Fig. 3*e–h*), we have simulated the olivine peak at 914 cm^{-1}. The robustness of our simulations is asserted by the small residual observed in Fig. 3*e–h*. For a theoretical proportion mixture of 0.80 and 0.20 weight fraction of olivine and gypsum, respectively (Fig. 3*d*), the calculated proportions (from equations 2 and 3) are 0.79 (0.08, error relative to simulations) for olivine and 0.21 (0.01) for gypsum (Fig. 3*h*). With a lower Ca-sulfate proportion, we obtain consistent results in between the measured and theoretical mixtures. For initial proportions at 0.90 and 0.10, we calculate 0.91 (0.01) for olivine and 0.09 (0) for gypsum (Fig. 3*c* and 3*g*). The same applies with the 0.01 and 0.05 mixtures of gypsum where 0.01 (0.01) and 0.06 (0) weight fraction of gypsum is calculated respectively, as shown in Fig. 3*a,b* and Fig. 3*e,f*.

The calculated coefficients from simulated areas in each mixture (see equation 3) as a function of the theoretical $CaSO_4$ content are shown in Fig. 4. The results are represented for the different mixtures with basaltic minerals: plagioclase–gypsum mixture in Fig. 4*a*; orthopyroxene–gypsum in Fig. 4*b*; and clinopyroxene and olivine–gypsum in Fig. 4*c* and 4*d*, respectively.

https://doi.org/10.1180/mgm.2018.147 Published online by Cambridge University Press

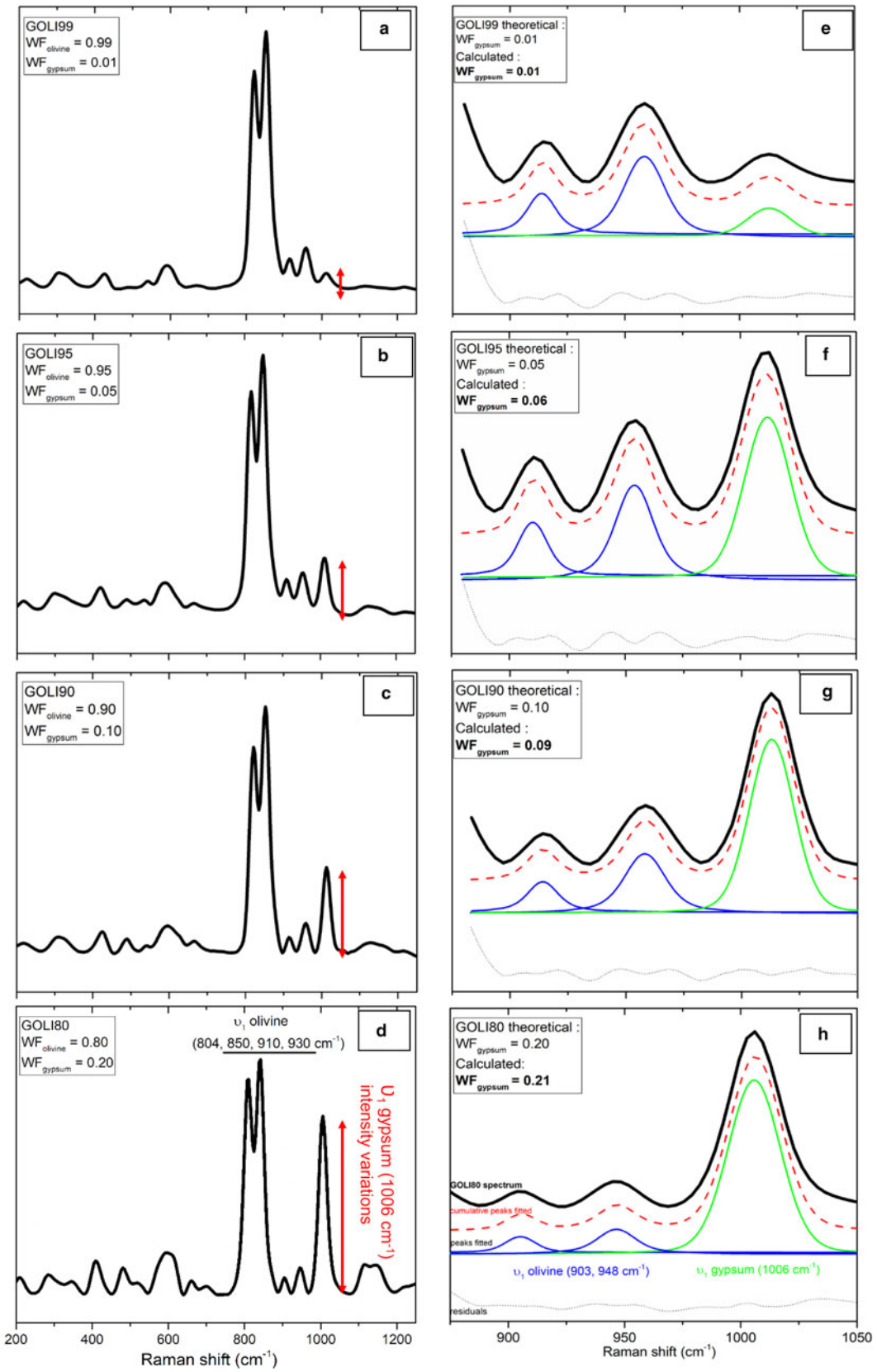

Fig. 3. Global spectra for every mixture of olivine with gypsum in different proportions: (*a*) $WF_{olivine} = 0.99$; (*b*) $WF_{olivine} = 0.95$; (*c*) $WF_{olivine} = 0.90$; and (*d*) $WF_{olivine} = 0.80$; with their main peaks reported. Variations of gypsum ν_1 (symmetric stretch of SO_4) peak intensity are shown as red arrows. Magnified (890–1100 cm^{-1} area) spectra acquired by Raman spectroscopy after mapping, from different mixtures of olivine with gypsum in several proportions: (*e*) $WF_{gypsum} = 0.01$; (*f*) $WF_{gypsum} = 0.05$; (*g*) $WF_{gypsum} = 0.10$; and (*h*) $WF_{gypsum} = 0.20$. Spectra are correlated with peak simulations: blue for olivine and green for gypsum. Red curves are cumulative peaks and black dotted lines are residuals from simulations. Weight fractions are calculated with peak simulations and reported in boxes in each graph and in Table 3.

https://doi.org/10.1180/mgm.2018.147 Published online by Cambridge University Press

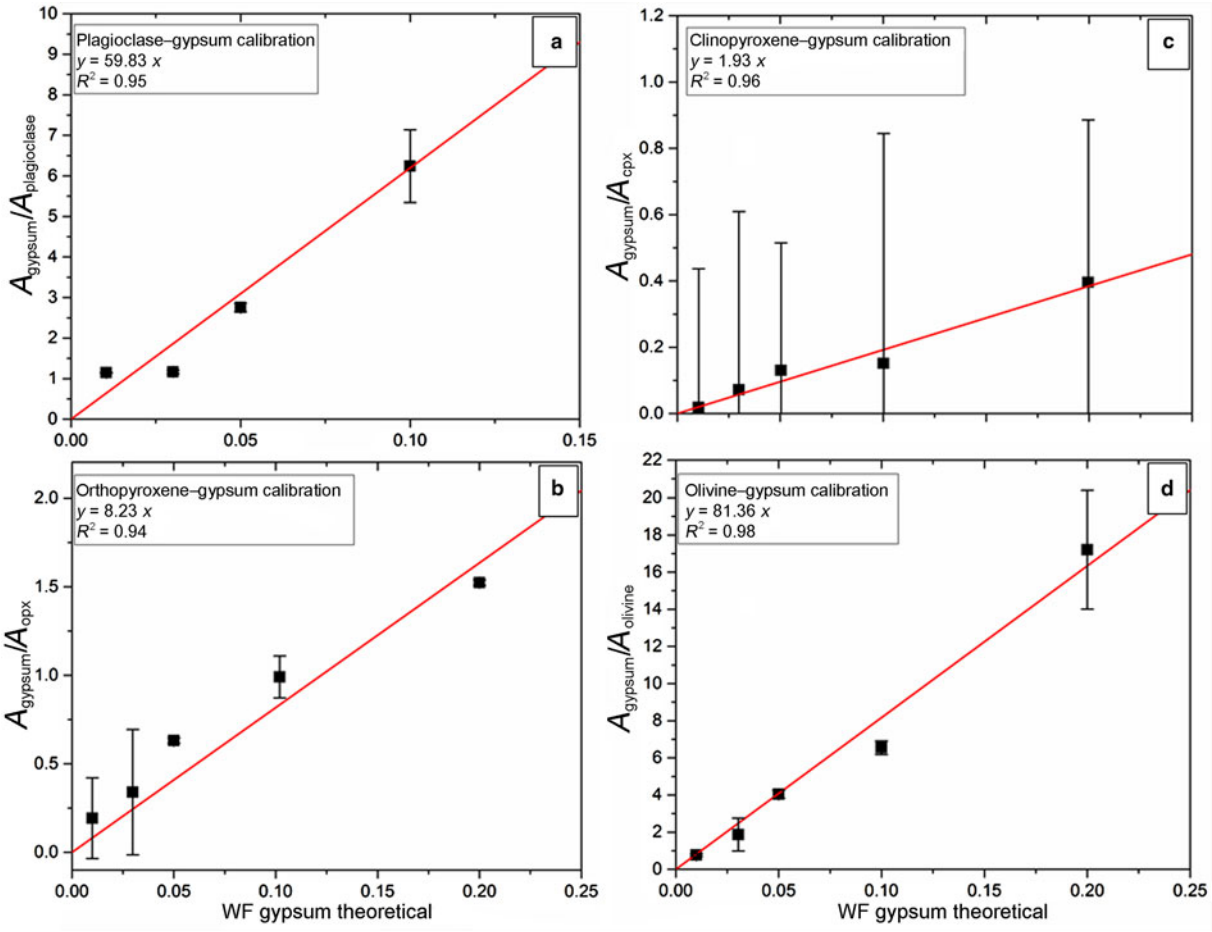

Fig. 4. Calibration coefficients calculated from simulated areas of gypsum and mineral mixes versus the theoretical weight fraction (WF) of gypsum. Black squares are simulated samples with their relative errors. Red lines correspond to calibration lines extrapolated from calibration coefficients depending on the theoretical weight fraction of gypsum. Calibration lines established on four binary mixtures of: (*a*) plagioclase; (*b*) orthopyroxene; (*c*) clinopyroxene; and (*d*) olivine; with gypsum in different proportions (WF_{gypsum} = 0.20, 0.10, 0.05, 0.03, 0.01). Equations and linear regression coefficient (R^2) of each calibration line are reported in boxes in each graph.

Results from simulations are reported in Table 3. In Fig. 4, we can observe that the best calibration (based on the linear regression coefficient R^2 which defines the quality of the linear regression on experimental data) is obtained for olivine–gypsum simulations compared to the calibration with other silicate minerals. Simulations (Figs 4*a* to 4*c*) show good R^2 with 0.95, 0.94 and 0.96 for plagioclase, orthopyroxene and clinopyroxene, respectively. The plagioclase mixture with 0.20 weight fraction of gypsum (i.e. GPG80, see Table 3) has been calibrated using different peaks because of the use of the 785 nm laser for our analysis. Consequently, this point is not reported in Fig. 4*a*.

We adopted the same procedure for ternary mixtures as for binary mixtures. The retained peak positions for our simulations are reported in Table 3. We considered the 300–390 cm^{-1} clinopyroxene peak areas, representative of Ca–O stretching vibrations, as they are isolated from the contribution of olivine and gypsum peaks in the Raman spectrum. For olivine, we consider the 947 cm^{-1}, one of SiO_4 symmetric stretching vibrations signatures, and 485 cm^{-1} for gypsum which represents the bending of SO_4 molecules. Those peaks were selected because they were the most separated from each other.

Simulation results and derived coefficients are reported in Table 3. We established a calibration expressed with the coefficient calculated (equation 3) from areas simulated for each mineral according to the initial weight fraction of gypsum, indicated in Fig. 5; we obtained a good calibration with $R^2 = 0.99$ on ternary mixtures.

Binary mixtures with Mg-sulfate

As for Ca-sulfate mixtures, we proceeded with the same method for pellets containing Mg-sulfate. Results are given from Mg-sulfate calibration on Fig. 6 where the same mixtures of natural silicate minerals of olivine, pyroxenes and plagioclase are represented. In Figs 6*a* and 6*c*, pyroxene calibration with Mg-sulfate are shown. The R^2 is fairly good (0.86 for orthopyroxene mixtures and 0.85 for clinopyroxene) and initial proportions of Mg-sulfate can be estimated satisfactorily from our method. Plagioclase mixtures with Mg-sulfate are reported on Fig. 6*b*, where we obtained R^2 = 0.43 and show less consistent results. Finally, olivine mixtures with initial proportions of Mg-sulfate (Fig. 6*d*) result in R^2 = 0.69. All results of calculated mixture proportions are reported in Table 3.

Discussion

Binary and ternary mixtures with sulfates were calibrated with several different proportions of sulfate. In this section, we discuss

https://doi.org/10.1180/mgm.2018.147 Published online by Cambridge University Press

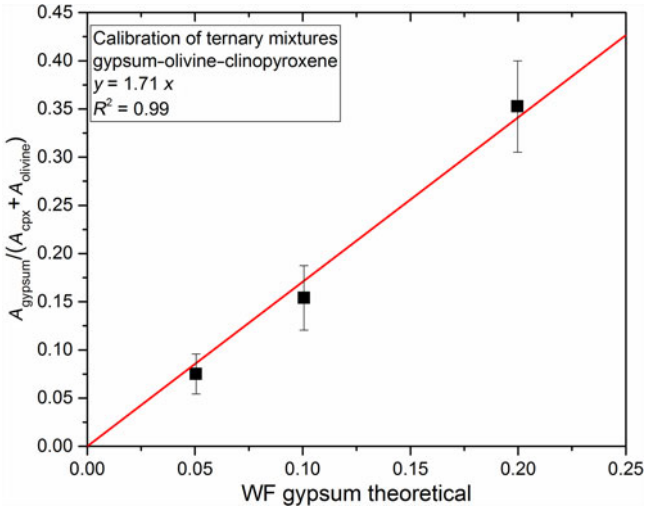

Fig. 5. Calibration line for ternary mixtures of gypsum (WF_{gypsum} = 0.2, 0.1, 0.05) with olivine ($WF_{olivine}$ = 0.40, 0.50, 0.50) and clinopyroxene ($WF_{clinopyroxene}$ = 0.40, 0.40, 0.45). Black squares are simulation results with errors (black vertical lines). Red line is the calibration line calculated from simulation results. Equation and regression linear coefficient (R^2) are specified in the graph box.

the limit of our calibration method and its application to the Martian context.

Detection limit of sulfur

In Fig. 4 we have reported results from binary mixtures of gypsum. We reported error bars extracted from errors under simulated peak areas. As can be observed in Figs 4*b* and 4*c*, corresponding to pyroxene-bearing mixtures, samples with 0.03 and 0.01 weight fractions of gypsum present a significant error in calculated values. Some selected peaks for the calibration do not exhibit a high Raman activity but we had to select those peaks, due to the necessity of choosing individual peaks for our simulations. In Table 3, we can see that we have still a good agreement between the calculated proportions and the initial proportions within the mixtures. Considering that some of molecule vibrations are less Raman active relative to Raman spectroscopy, we consider that our method of calibration is reliable until $WF_{sulfate}$ = 0.03 weight fraction in a mechanical mixture.

Knowing this detection limit for our calibration, we can extrapolate this method to Martian rocks. With the proposed method and the calibration equations, S could be determined at the surface of Mars for a sedimentary rock containing sulfate

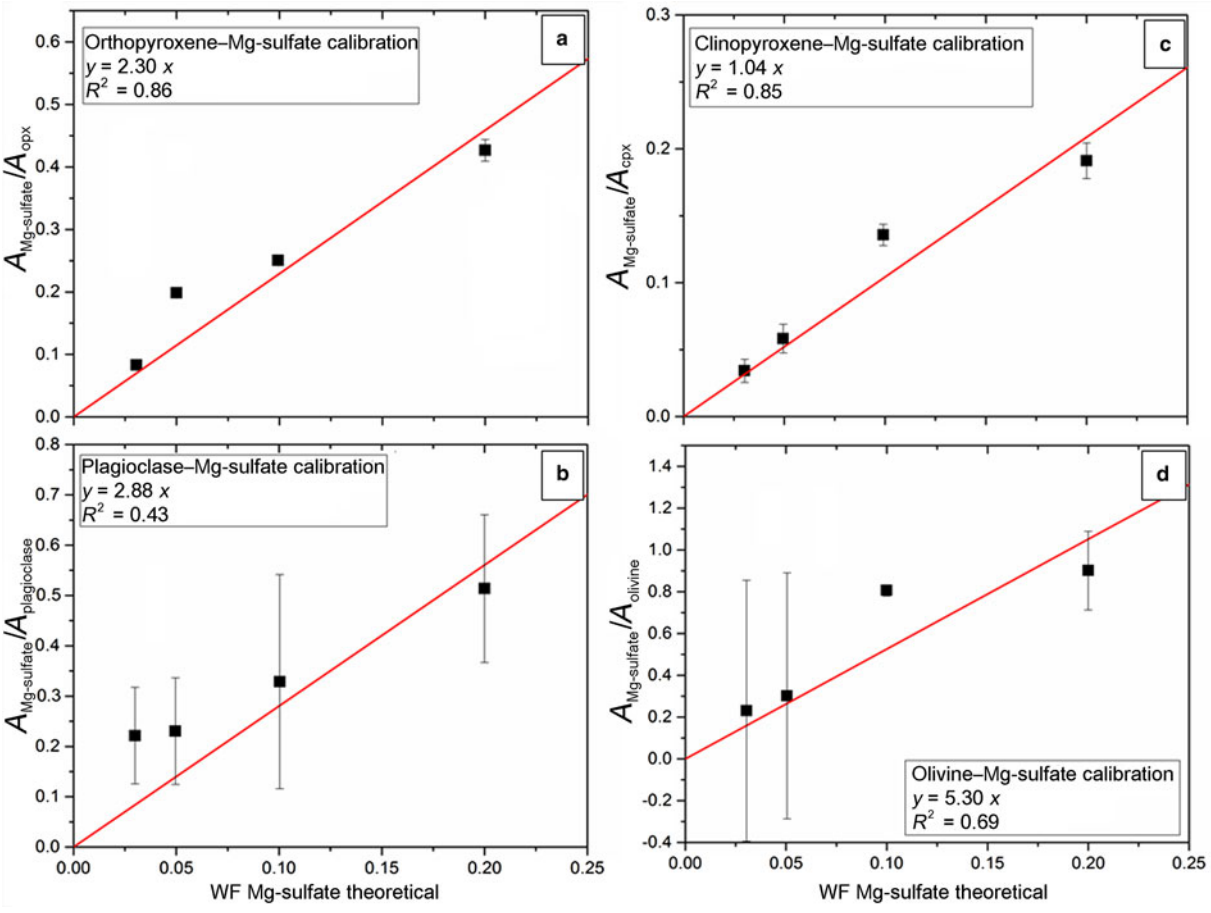

Fig. 6. Calibration coefficients calculated from simulated areas of Mg-sulfate and mineral mixes versus the theoretical weight fraction (WF) of the sulfate. Black squares are simulated samples with their relative errors. Red lines correspond to calibration lines extrapolated from calibration coefficients depending on theoretical weight fraction of Mg-sulfate. Calibration lines established on four binary mixtures of: (*a*) orthopyroxene; (*b*) plagioclase; (*c*) clinopyroxene; and (*d*) olivine; with Mg-sulfate in different proportions (WF_{gypsum} = 0.20, 0.10, 0.05 and 0.03). Equations and linear regression coefficients (R^2) of each calibration lines are reported in boxes for every graph.

https://doi.org/10.1180/mgm.2018.147 Published online by Cambridge University Press

until WF_S = ~0.007 weight fraction (i.e. 7000 ppm). Below this S content, our calibration can still be applied, but the errors will be higher and results might not be reliable.

Application of the calibration curves to the determination of sulfur on the Martian surface

The calibration results for all the mixtures created are given in Fig. 7, showing the good agreement of our calibration method. This plot shows that the calculated proportions of gypsum are close to the theoretical proportions and all data points are aligned along the 1:1 line. Ternary mixtures with gypsum are also represented and are in good accordance. Mg-sulfate mixtures in Fig. 7 also show that the calibration is good and data points are aligned along the 1:1 line.

All the calibration equations calculated from our calibration method for gypsum and Mg-sulfate mixtures are reported in Table 3.

As a result, we can determine the sulfate content in a mixture with olivine, pyroxenes and plagioclase in unknown proportions according to equations extracted from our simulations shown in Figs 4, 5 and 6. Using a Raman spectrum obtained on the surface of Mars of a mechanical solid mixture containing sulfate (Ca or Mg), and simulating specific peaks (reported in Table 3), a coefficient can be calculated (i.e. the '*a*' component in the equations in Table 3).

The calibration method established in present study based on Raman spectroscopy will be of use for the 2020 Mars mission to quantify S abundance when present as sulfates. However, the peak selections from a Raman spectrum must be conducted with care. We suggest using only the peaks mentioned in the present work and reported in the Supplementary Table S1. However, this will be dependent on the resolution of the SuperCam Raman spectrometer and the quality of the acquired signal (Wiens *et al.*, 2016). In the case of a low resolution, peaks with low intensities (for instance ν_3) will be difficult to constrain. However, other peaks mentioned in the Supplementary Table S1, such as ν_1 or ν_2 can be defined sufficiently well by the future rover and calibration can still be applicable (see peak information in Supplementary Table S1). As our analyses were performed with a high-resolution Raman spectrometer, further analyses will be acquired with a pulsed-Raman with distance from the sample similar to the one presupposed for SuperCam in order to compare data and modify, if necessary, the calibration.

Furthermore, Mars mineralogy has been partly investigated using remote sensing and rover data, as well as Martian meteorites, showing that pigeonite and augite are the two most common pyroxenes found in Martian rocks (both are clinopyroxenes but with low Ca content for pigeonite) (e.g. Lodders 1998, Agee and Draper 2004; Mustard *et al.*, 2005; Cousin *et al.*, 2017; Morrison *et al.*, 2018). Mg-rich olivine, orthopyroxene and plagioclase have also been detected in Martian meteorites and at the surface of the planet (Agee and Draper 2004; Mustard *et al.*, 2005; Dehouck *et al.*, 2014; Cousin *et al.*, 2017; Morrison *et al.*, 2018). Nonetheless, Fe-rich olivine can be expected in small amounts which only differs in spectral signature by the relative intensity between the double peak around 800–850 cm^{-1}. As our calibration is not based on those peaks (see Table 3), the quantification of sulfate with fayalite can still be possible. Plagioclase such as anorthite may be the most common feldspar on Mars (Bish *et al.*, 2013; Blake *et al.*, 2013; Vaniman *et al.*, 2017) although andesine has been observed as the predominant plagioclase at Gale crater by the Curiosity rover instruments (Sautter *et al.*, 2016; Morrison *et al.*, 2018). Consequently, the proposed calibration method can be useable for a mixture of sedimentary rocks containing sulfates and silicate minerals even if the minerals present do not have the same composition within a solid solution as used in our study.

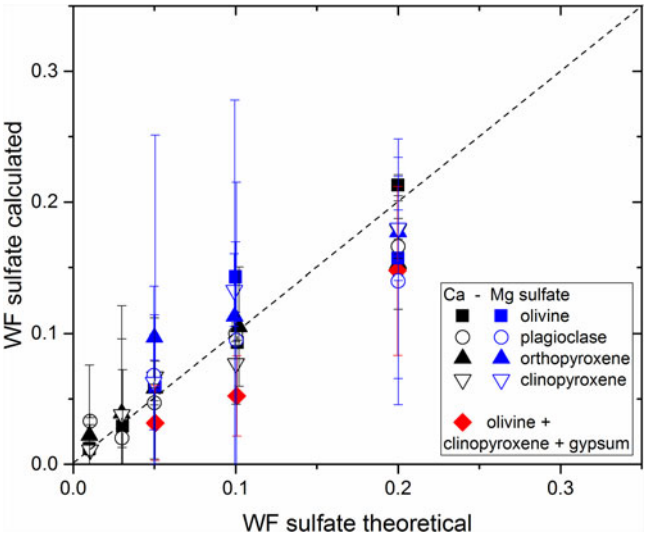

Fig. 7. Weight fractions calculated for sulfates (Ca- and Mg-sulfate) depending on its theoretical weight fraction in each mixture of olivine, clinopyroxene, orthopyroxene and plagioclase. Black = gypsum binary samples; blue = Mg-sulfate mixtures; red diamonds = ternary mixtures of gypsum.

Summary

In the present investigation, we have prepared pellets by mixing Ca and Mg sulfates with silicate minerals commonly found in basalt (olivine, pyroxenes and plagioclase) in order to investigate the Raman signature of polymineralic mechanical assemblages. The main objective was to establish a relevant calibration for the determination of S content at the surface of Mars with analytical conditions close to the future Raman spectrometer on SuperCam equipment for the 2020 spatial mission. Calibration equations were obtained for both binary and ternary mixtures of $CaSO_4$ with minerals for a range of gypsum weight fractions (0.01 to 0.20). Equations were also estimated from Mg-sulfate mixtures with initial proportions of 0.03 to 0.20 weight fraction.

The protocol used in this study involves simulations of the resulting average Raman spectrum using a Voigt distribution on peaks attributed to each mineral. The simulation of the entire Raman spectrum does not have good enough accuracy and careful attention is necessary for peak identifications. The actual method could be applied to the quantitative characterisation of the soil of Mars which is known to contain sedimentary rocks containing sulfates and silicate minerals obtained from bedrock erosion.

Given our equations extracted from calibrations on both Mg and Ca sulfates, we would be able to calculate a coefficient from a given Raman spectrum acquired on Mars and treated according to specific peak simulations. Coupling this coefficient with the proper calibration equation (i.e. when knowing the mineralogical characterisation of the mixture analysed) we can estimate the proportion of this sulfate in the weight fraction. By extent, this calibration could be used to constrain part of the S content at the surface carried by sulfate mineral phases. We have estimated the detection limit of S at 7000 ppm which is well below the current detection limit by the LIBS technique (e.g. Wiens *et al.*, 2012;

https://doi.org/10.1180/mgm.2018.147 Published online by Cambridge University Press

Nachon, 2016; Nachon *et al.*, 2017; Anderson *et al.*, 2017). Nevertheless, further calibrations are required involving more complex mineral mixtures, including other sulfates (Fe-sulfate) and sulfides, and mixtures with more than four compounds. Calibration using a Martian basalt glass analogue in the presence of sulfates could also be established to better constrain the S quantification on the surface of Mars.

Acknowledgements. We thank particularly the Université de Nantes, the LPG and Institut des Matériaux de Nantes Jean Rouxel for their support with experimental and analytical facilities. We also thank Jean Pierre Lorand (LPG) for providing the rocks used in our samples. We acknowledge the support of the Centre National d'Etudes Spatiales (CNES), the Région Pays de la Loire and the Agence Nationale de la recherche (ANR) under the contract ANR-16-CE31-0012 entitled "Mars-PRIME".

Supplementary material. To view Supplementary material for this article, please visit https://doi.org/10.1180/mgm.2018.147

References

Agee C.B. and Draper D.S. (2004) Experimental constraints on the origin of Martian meteorites and the composition of the Martian mantle. *Earth Planet Science Letters*, **224**, 415–429.

Anderson D.E., Ehlmann B.L., Forni O., Clegg S.M., Cousin A., Thomas N.H. *et al.* (2017) Characterization of LIBS estimation lines for the identification of chlorides, carbonates, and sulfates in salt/basalt mixtures for the application to MSL ChemCam data. *Journal of Geophysical Research: Planets*, **122**, 744–770.

Arvidson R.E., Poulet F., Bibring J.-P., Wolff M., Gendrin A., Morris R.V., Freeman J.J., Langevin Y., Mangold N. and Bellucci G. (2005) Spectral reflectance and morphologic correlations in Eastern Terra Meridiani, Mars. *Science*, **307**, 1591–1594.

Bandfield J.L., Hamilton V.E. and Christensen P.R. (2000) A global view of Martian surface composition from MGS-TES. *Science*, **287**, 1626–1630.

Baratoux D., Toplis M.J., Monnereau M. and Sautter V. (2013) The petrological expression of early Mars volcanism. *Journal of Geophysical Research: Planets*, **118**, 59–64.

Bish D.L., Blake D.F., Vaniman D.T., Chipera S.J., Morris R.V., Ming D.W., Treiman A.H., *et al.* (2013) X-ray diffraction results from Mars Science Laboratory: Mineralogy of Rocknest at Gale Crater. *Science*, **341**, Issue 6153, 1238932.

Bishop J.L., Lane M.D., Dyar M.D., King S.J., Brown A.J. and Swayze G. (2014) Spectral properties of Ca-sulfates: Gypsum, Bassanite and Anhydrite. *American Mineralogist*, **99**, 2105–2115.

Blake D.F., Morris R.V., Kocurek G., Morrison S.M., Downs R.T., Bish D., Ming D.W., *et al.* (2013) Curiosity at Gale crater, Mars: Characterization and analysis of the Rocknest sand shadow. *Science*, **341**, Issue 6153, 1239505.

Brawer S.A. and White W.B. (1975) Raman spectroscopic investigation of the structure of silicate glasses. I. The binary alkali silicates. *The Journal of Chemical Physics*, **63**, 2421.

Bremard C., Dhamelincourt P., Laureyns J. and Turrell G. (1986) Polarization measurements in micro-Raman and microfluorescence spectrometries. *Journal of Molecular Structure*, **142**, 13–16.

Buzgar N., Buzatu A. and Sanislav I.V. (2009) The Raman study on certain sulfates. *Analele Ştiinţifice ale Universităţii „AL. I. Cuza" Iaşi, seria Geologie*, **55**(1), 5–23.

Carter J., Poulet F., Bibring J.-P., Mangold N. and Murchie S. (2013) Hydrous minerals on Mars as seen by the CRISM and OMEGA imaging spectrometers: Updated global view. *Journal of Geophysical Research: Planets*, **118**, 1–28.

Chopelas A. (1991) Single crystal Raman spectra of forsterite, fayalite, and monticellite. *American Mineralogist*, **76**, 1101–1109.

Clegg S.M., Wiens R.C., Dyar M.D., Vaniman D.T., Thompson J.R., Sklute E.C., *et al.* (2007) Sulfur geochemical analysis with remote laser-induced breakdown spectroscopy on the 2009 Mars science laboratory rover. *Lunar Planetary Science Conference XXXVIII*, abstract #1960. [Lunar and Planetary Institute abstracts available at https://www.lpi.usra.edu/publications/absearch/]

Cousin A., Sautter V., Payré V., Forni O., Mangold N., Gasnault O., Le Deit L., Johnson J., Maurice S., Salvatore M., Wiens R.C., Gasda P. and Rapin W. (2017) Classification of igneous rocks analysed by ChemCam at Gale Crater, Mars. *Icarus*, **288**, 265–283.

Culka A., Košek F., Drahota P., Jehlička J. (2014) Use of miniaturized Raman spectrometer for detection of sulfates of different hydration states – Significance for Mars studies. *Icarus*, **243**, 440–453.

Dehouck E., McLennan S.M., Meslin P.-Y. and Cousin A. (2014) Constraints on abundance, composition, and nature of X-ray amorphous components of soils and rocks at Gale crater, Mars. *Journal of Geophysical Research: Planets*, **119**, 2640–2657.

Delhaye M. and Dhamelincourt P. (1975) Raman microprobe and microscope with laser excitation. *Journal of Raman spectroscopy*, **3**, 33–43.

Dubessy J., Caumon M.-C., Rull F. and Sharma S. (2012) Instrumentation in Raman spectroscopy: elementary theory and practice. Pp. 83–172 in: *Raman Spectroscopy Applied to Earth Sciences and Cultural Heritage* (J. Dubessy, M.-C. Caumon and F. Rull, editors). EMU Notes in Mineralogy, **12**.

Ehlmann B.L., Berger G., Mangold N., Michalski J.R., Catling D.C., Ruff S.W., Chassefière E., Niles P.B., Chevrier V. and Poulet F. (2013) Geochemical consequences of widespread clay mineral formation in Mars' ancient crust. *Space Science Reviews*, **174**, 329–364.

Forni O., Gaft M., Toplis M.J., Clegg S.M., Maurice S., Wiens R.C., *et al.* (2015) First detection of fluorine on Mars: Implications for Gale Crater's geochemistry. *Geophysical Research Letters*, **42**, 1020–1028.

Fouchet T., Wiens R., Maurice S., Johnson J.R., Clegg S., *et al.* (2016) The SuperCam Remote Sensing Suite for MARS 2020: Nested and Co-Aligned LIBS, Raman, and VISIR Spectroscopies, and color micro-imaging. *Division for Planetary Sciences and the European Planetary Science Congress Oct 2016, Pasadena, United States*. American Astronomical Society, 48, pp.123.09, 2016.

Freeman J.J., Wang A., Kuebler K.E., Jolliff D.L. and Haskin L.A. (2008) Characterization of natural feldspars by Raman spectroscopy for future planetary exploration. *The Canadian Mineralogist*, **46**, 1477–1500.

Gendrin A., Mangold N., Bibring J.P., Langevin Y., Gondet B., Poulet F., Bonello G., Quantin C., Mustard J., Arvidson R. and LeMouélic S. (2005) Sulfates in Martian layered terrains: the OMEGA/Mars express view. *Science*, **307**, 1587–1591.

Hoehse M., Mory D., Florek S., Weritz F., Gornushkin I. and Panne U. (2009) A combined laser-induced breakdown and Raman spectroscopy Echelle system for elemental and molecular microanalysis. *Spectrochimica Acta Part B: Atomic Spectroscopy*, **64**, 1219–1227.

Huang E., Chen C.H., Huang T., Lin E.H. and XU J.-A. (2000) Raman spectroscopic characteristics of Mg-Fe-Ca pyroxenes. *American Mineralogist*, **85**, 473–479.

Jehlicka J., Vitek P., Edwards H.G.M, Heagraves M. and Capoun T. (2009) Application of portable Raman instruments for fast and non-destructive detection of minerals on outcrops. *Spectrochimica Acta Part A*, **73**, 410–419.

King P.L. and McLennan S.M. (2010) Sulfur on Mars. *Elements*, **6**, 107–112.

Knittle E., Phillips W. and Williams Q. (2001) An infrared and Raman spectroscopic study of gypsum at high pressures. *Physics Chemistry Mineral*, **28**, 630–640.

Kontoyannis C.G., Orkoula M.G. and Koutsoukos P.G. (1997) Quantitative analysis of sulfated calcium carbonates using Raman spectroscopy and x-ray power diffraction. *The Analyst*, **122**, 33–38.

Kolesov B.A. and Geiger C.A. (2004) A Raman spectroscopic study of Fe-Mg olivines. *Physics and Chemistry Minerals*, **31**, 142–154.

Kolesov B.A. and Tanskaya J.V. (1996) Raman spectra and cation distribution in the lattice of olivines. *Materials Research Bulletin*, **31**, 1035–1044.

Kristova P., Hopkinson L., Rutt K., Hunter H. and Cressey G. (2013) Quantitative analyses of powdered multi-minerallic carbonate aggregates using a portable Raman spectrometer. *American Mineralogist*, **98**, 401–409.

Kuebler K.E., Jolliff B.L., Wang A. and Haskin L.A. (2006) Extracting olivine (Fo-Fa) compositions from Raman spectral peak positions. *Geochimica et Cosmichimica Acta*, **70**, 6201–6222.

Lodders K. (1998) A survey of shergottite, nakhlite and chassigny meteorites whole-rock compositions. *Meteoritics & Planetary Science*, **33**, 183–190.

Le Losq C., Neuville D.R, Moretti R. and Roux J. (2012) Determination of water content in silicate glasses using Raman spectrometry: Implications for the study of explosive volcanism. *American Mineralogist*, **97**, 779–790.

Mangold N., Baratoux D., Witasse O., Encrenaz T. and Sotin C. (2016) Mars: a small terrestrial planet. *Astronomy and Astrophysics Review*, **24**, 15.

Mangold N., Schmidt M.E., Fisk M.R., Forni O., McLennan S.M., Ming D.W., Sautter V., Sumner D., Williams A.J., Clegg S.M., Cousin A., Gasnault O., Gellert R., Grotzinger J.P. and Wiens R.C. (2017) Classification scheme for sedimentary and igneous rocks in Gale crater, Mars. *Icarus*, **284**, 1–17.

Maurice S., Wiens R.C., Saccoccio M., Barraclough B., Gasnault O. and 65 more authors (2012) The ChemCam Instrument Suite on the Mars Science Laboratory (MSL) Rover: Science objectives and Mast Unit Description. *Space Science Reviews*, **170**, 167–227.

Maurice S., Clegg S.M., Wiens R.C., Gasnault O., Rapin W., Forni O., Cousin A., *et al.* (2016) ChemCam activities and discoveries during the nominal mission of Mars Science Laboratory in Gale crater, Mars. *Journal of Analytical Atomic Spectrometry*, **31**, 863–889.

McKeown D.A., Bell M.I. and Caracas R. (2010) Theoretical determination of the Raman spectra of single-crystal forsterite (Mg_2SiO_4). *American Mineralogist*, **95**, 980–986.

McLennan S.M., Bell J., Calvin W.M., Christensen P., Clark B.C., de Souza P.A., Farmer J., *et al.* (2005) Provenance and diagenesis of the evaporite-bearing Burns formation, Meridiani Planum, Mars. *Earth and Planetary Science Letters*, **240**, 95–121.

McMillan P. (1984) Structural studies of silicate glasses and melts: applications and limitations of Raman spectroscopy. *American Mineralogist*, **69**, 622–644.

McSween H.Y., Taylor G.J. and Wyatt M.B. (2009) Elemental composition of the Martian crust. *Science*, **324**, 736–739.

Mercier M., Di Muro A., Giordano D., Métrich N., Lesne P., Pichavant M., Scaillet B., Clocchiatti R. and Montagnac G. (2009) Influence of glass polymerization and oxidation on micro-Raman water analysis in alumino-silicate glasses. *Geochimica et Cosmochimica Acta*, **73**, 197–217.

Meslin P.-Y., Gasnault O., Forni O., Schröder S., Cousin A., 55 more authors and the MSL Science Team (2013) Soil diversity and hydration as observed by ChemCam at Gale Crater, Mars. *Science*, 341.

Morizet Y., Brooker R.A., Iacono-Marziano G. and Kjarsgaard B.A. (2013*a*) Quantification of dissolved CO_2 in silicate glasses using micro-Raman spectroscopy. *American Mineralogist*, **98**, 1788–1802.

Morizet Y., Paris M., Di Carlo I. and Scaillet B. (2013*b*) Effect of Sulphur on the structure of silicate melts under oxidizing conditions. *Chemical Geology*, **358**, 131–147.

Morizet Y., Gennaro E., Jego S., Zajacz Z., Iacono-Marziano G., Pichavant M., Di Carlo I., Ferraina C. and Lesne P. (2017) A Raman calibration for the quantification of SO_4^{2-} groups dissolved in silicate glasses: Application to natural melt inclusions. *American Mineralogist*, **102**, 2065–2076.

Morrison S.M. (2018) Crystal chemistry of Martian minerals from Bradbury Landing through Naukluft Plateau, Gale Crater, Mars. *American Mineralogist*, **103**, 857–871.

Mustard J.F., Poulet F., Bibring J.P., Langevin Y., Gondet B., Mangold N., Bellucci G. and Altieri F. (2005) Olivine and pyroxene diversity in the crust of Mars. *Science*, **307**, 1594–1597.

Mysen B.O. and Virgo D. (1980*a*) Solubility mechanisms of carbon dioxide in silicate melts: a Raman spectroscopic study. *American Mineralogist*, **65**, 885–899.

Mysen B.O. and Virgo D. (1980*b*) The solubility behavior of CO_2 in melts on the join $NaAlSi_3O_8$–$CaAl_2SiO_8$–CO_2 at high pressures and temperatures: A Raman spectroscopic study. *American Mineralogist*, **65**, 1166–1175.

Nachon M. (2016) *Chimie de la surface de Mars dans le cratère Gale par l'analyse de données élémentaires de ChemCam sur Curiosity couplée à des simulations en laboratoire*. PhD thesis, Université de Nantes, France.

Nachon M., Mangold N., Forni O., Kah L.C., Cousin A., Wiens R.C., Anderson R., *et al.* (2017) Chemistry of diagnetic features analyzed by ChemCam at Pahrump Hill, Gale crater, Mars. *Icarus*, **281**, 131–136.

Noguchi N., Shinoda K. and Masuda K. (2009) Quantitative analysis of binary mineral mixtures using Raman microspectroscopy: Calibration curves for silica and calcium carbonate minerals and application to an opaline silica nodule of volcanic origin. *Journal of Mineralogical and Petrological Sciences*, **104**, 253–262.

Ody A. (2012) *Dépouillement et interprétation des données spatiales d'imagerie hyperspectrale de Mars (OMEGA/MEx) Evolution volcanique de la surface de Mars*. PhD thesis. Université Paris Sud - Paris XI.

Ollila A.M., Wiens R.C., Perez R., Nelson A., Bodine M., Maurice S., Sharma S., *et al.* (2017) Preliminary evaluation of the Mars 2020 Rover's SuperCam Development Unit: co-aligned chemical and mineralogical analyses. *Lunar Planetary Science Conference XLVIII*, abstract #2339. [Lunar and Planetary Institute abstracts available at https://www.lpi.usra.edu/publications/absearch/]

Panczer G., De Ligny D., Mendoza C., Gaft M., Seydoux-Guillaume A.-M. and Wang X. (2012) Raman and fluorescence. Pp. 1–22 in: *Raman Spectroscopy Applied to Earth Sciences and Cultural Heritage* (J. Dubessy, M.-C. Caumon and F. Rull, editors). EMU Notes in Mineralogy, **12**.

Poulet F., Bibring J.-P., Mustard J.F., Gendrin A., Mangold N., Langevin Y., Arvidson R.E., Gondet B., Gomez C., *et al.* (2005) Phyllosilicates on Mars and implications for early Martian climate. *Nature*, **438**, 623–627.

Prencipe M., Mantovani L., Tribaudino M., Bersani D. and Lottici P.P. (2011) The Raman spectrum of diopside: a comparison between ab initio calculated and experimentally measured frequencies. *European Journal of Mineralogy*, **24**, 457–464.

Reynard B., Montagnac G. and Cardon H. (2012) Raman spectroscopy at high pressure and temperature for the study of the Earth's mantle and planetary minerals. Pp. 365–388 in: *Raman Spectroscopy Applied to Earth Sciences and Cultural Heritage* (J. Dubessy, M.-C. Caumon and F. Rull, editors). EMU Notes in Mineralogy, **12**.

Rossano S. and Mysen B. (2012) Raman spectroscopy of silicate glasses and melts in geological systems. Pp. 319–364 in: *Raman spectroscopy applied to Earth Sciences and Cultural Heritage* (J. Dubessy, M.-C. Caumon and F. Rull, editors). EMU Notes in Mineralogy, **12**.

Rull F. (2012) The Raman Effect and the vibrational dynamics of molecules and crystalline solids. Pp. 1–60 in: *Raman Spectroscopy Applied to Earth Sciences and Cultural Heritage* (J. Dubessy, M.-C. Caumon and F. Rull, editors). EMU Notes in Mineralogy, **12**.

Sallé B., Lacour J-L., Vors E., Fichet P., Maurice S., Cremers D.A. and Wiens R.C. (2004) Laser-Induces Breakdown Spectroscopy for Mars surface analysis: capabilities at stand-off distances and detection of chlorine and sulfur elements. *Spectrochimica Acta Part B: Atomic Spectroscopy*, **59**, 1413–1422.

Sautter V., Toplis M.J., Wiens R.C., Cousin A., Fabre C., Gasnault O., Maurice S., *et al.* (2015) In situ evidence for continental crust on early Mars. *Nature Geosciences*, **8**, 605–609.

Sautter V., Toplis M.J., Beck P., Mangold N., Wiens R., Pinet P., Cousin A., Maurice S., *et al.* (2016) Magmatic complexity on early Mars as seen through a combination of orbital, in-situ and meteorite data. *Lithos*, **254–255**, 36–52.

Sharma S.K., Simons B. and Yoder Jr H.S. (1983) Raman study of anorthite, calcium Tschermak's pyroxene, and gehlnite in crystalline and glassy states. *American Mineralogist*, **68**, 11–12.

Squyres S.W. and Knoll A.H. (2005) Sedimentary rocks at Meridiani Planum: Origin, diagenesis and implications for life on Mars. *Earth Planetary Science Letters*, **240**, 1–10.

Stolper E.M., Baker M.B., Newcombe M.E., Schmidt M.E., Treiman A.H., Cousin A., Dyar M.D. *et al.* (2013) The petrochemistry of Jake_M: Martian mugearite. *Science*, **341**, Issue 6153, 1239463.

Tarcea N. and Popp J. (2012) Raman data analysis. Pp. 195–228 in: *Raman Spectroscopy Applied to Earth Sciences and Cultural Heritage* (J. Dubessy, M.-C. Caumon and F. Rull, editors). EMU Notes in Mineralogy, **12**.

Taylor S.R. and McLennan S.M. (editors) (2009) *Planetary Crusts. Their Composition, Origin and Evolution*. Cambridge University Press, UK. pp. 378.

Tribaudino M., Mantovani L., Bersani D. and Lottici P.P. (2012) Raman spectroscopy of $(Ca,Mg)MgSi_2O_6$ clinopyroxenes. *American Mineralogist*, **97**, 1339–1347.

Vaniman D.T, Martínez G.M., Rampe E.B., Bristow T.F., Blake D.F., *et al.* (2017) Calcium sulfates at Gale Crater and limitations on gypsum stability. *Lunar Planetary Science Conference XLVIII*, abstract #1661. [Lunar and

https://doi.org/10.1180/mgm.2018.147 Published online by Cambridge University Press

Planetary Institute abstracts available at https://www.lpi.usra.edu/publications/absearch/]

Wang A., Jolliff B.L., Haskin L.A., Kuebler K.E. and Viskupic K.M. (2001) Characterization and comparison of structural and compositional features of planetary quadrilateral pyroxenes by Raman spectroscopy. *American Mineralogist*, **86**, 790–806.

Wiens R.C., Maurice S., Barraclough B., Saccoccio M., Barkley W.C., Bell III J.F. *et al.* (2012) The ChemCam instrument suite on the Mars Science Laboratory (MSL) Rover: body unit and combined system tests. *Space Science Reviews*, **170**, 167–227.

Wiens R.C., Maurice S., Rull F. and the SuperCam Team (2016) SuperCam remote-sensing on the Mars 2020 Rover: Science goals and overview. *3rd International Workshop on Instrumentation for Planetary Missions*. Abstract #4136.

Wray J., Hansen S.T., Dufek J., Swayze G.A., Murchie S.L., Seelos F.P., Skok J.R., Irwin III R.P. and Ghiorso M.S. (2013) Prolonged magmatic activity on Mars inferred from the detection of felsic rocks. *Nature Geoscience*, **6**, 1013–1017.

Zajacz Z., Halter W., Malfait W.J., Bachmann O., Bodnar R.J., Hirschmann M.M., Mandeville C.W., Morizet Y., Müntener O., Ulmer P. and Webster J.D. (2005) A composition-independent quantitative determination of the water content in silicate glasses and silicate melt inclusions by confocal Raman spectroscopy. *Contributions to Mineralogy and Petrology*, **150**, 631–642.

https://doi.org/10.1180/mgm.2018.147 Published online by Cambridge University Press